UDK 532.5; 544.452.42

Ye. Belyayev*, A. Kaltayev

Faculty of Mechanics and Mathematics, al-Farabi Kazakh National University, Almaty, Kazakhstan
*e-mail:: yerzhan.belyayev@gmail.com

Numerical study of supersonic turbulent free shear layer

Abstract. Numerical study of two-dimensional supersonic turbulent free shear layer is performed. The system of Favre-Averaged Naveir-Stokes equations for multispecies flow is solved using ENO scheme of third-order in accuracy. The k-ε two-equation turbulence models with compressibility correction are applied to calculate the eddy viscosity coefficient. In order to produce the roll-up and pairing of vortex rings, an unsteady boundary condition is applied at the inlet plane. At the outflow, the non-reflecting boundary condition is taken. The obtained results are compared with available experimental data.
Keywords: supersonic free shear flow, mixing layer, ENO-scheme, k-ε model, compressibility.

Introduction

Compressible mixing layer is an important flow in extensive engineering applications. In particular, the shear layer configuration is a simple and yet fundamental to understand how fuel flow will mix and combust with supersonic oxidizer flow in SCRAM jet engines combustion chambers of hypersonic vehicles. As is well known the main objectives of investigating the physical processes in combustion chamber of these engines is aimed to maximize thrust by enhancing the fuel-air mixing and combustion.

It is necessary to take into account the influence of gas-dynamical structure, turbulence effects and chemical reactions for understanding physical structure of fuel-air mixture combustion in numerical model. Studying combustion in shear layer requires accurate predictions of mixing and combustion efficiency to which special attention should be paid to simulation the unsteady behavior of mixing layer roll-up and vortex formation. The gas-dynamical structure of mixing between two parallel super-subsonic flows has been comprehensively studied by many investigators. Nowadays, there are a large number of works on experimental [1-9], analytical [10-11] and numerical [12-27] study of this problem in the view of above physical effects as separately as with including all of them. Experimental efforts investigating the roll of large scale structures and growth mechanisms in compressible mixing layer have been done in sufficient details by researchers [1-6]. There are a great deal of researches devoted to the turbulence problem and influence of turbulence quantities on the mixing and vorticity formation [7-9].

The behavior of shear layers of perfect gases have been entirely realized in mathematical models, but the practical design of supersonic ramjet (scramjet) engines requires the shear layer growth enhancements for multispecies gases. Successful numerical models of such flows with the detail flow physics represent a difficult problem. Therefore the investigators studied some physical phenomena separately or proposed the numerical method, which are important for solution of this complex system. In [12, 15-16] have been modeled the free shear layer flowfield structures using the system of compressible Euler equations. For example, in [12] have been numerically studied the supersonic-subsonic free shear layer applying high order WENO scheme to the system of 2D axisymmetric Euler equations and numerical turbulence model taken as a SGS model. During numerical experiment revealed that at high-convective Mach number turbulence mixing rates reduces and vortex roll-up and pairing suppresses. In [13-14, 17] have been performed numerical experiment based on the system of Navier-Stokes equations for monatomic (air) gas to study the growth of instabilities in supersonic free shear layers. Xiao-Tian Shi et al. [17] conducted numerical simulations of compressible mixing layers based on discontinuous Galerkin me-

 Printed in Kazakhstan

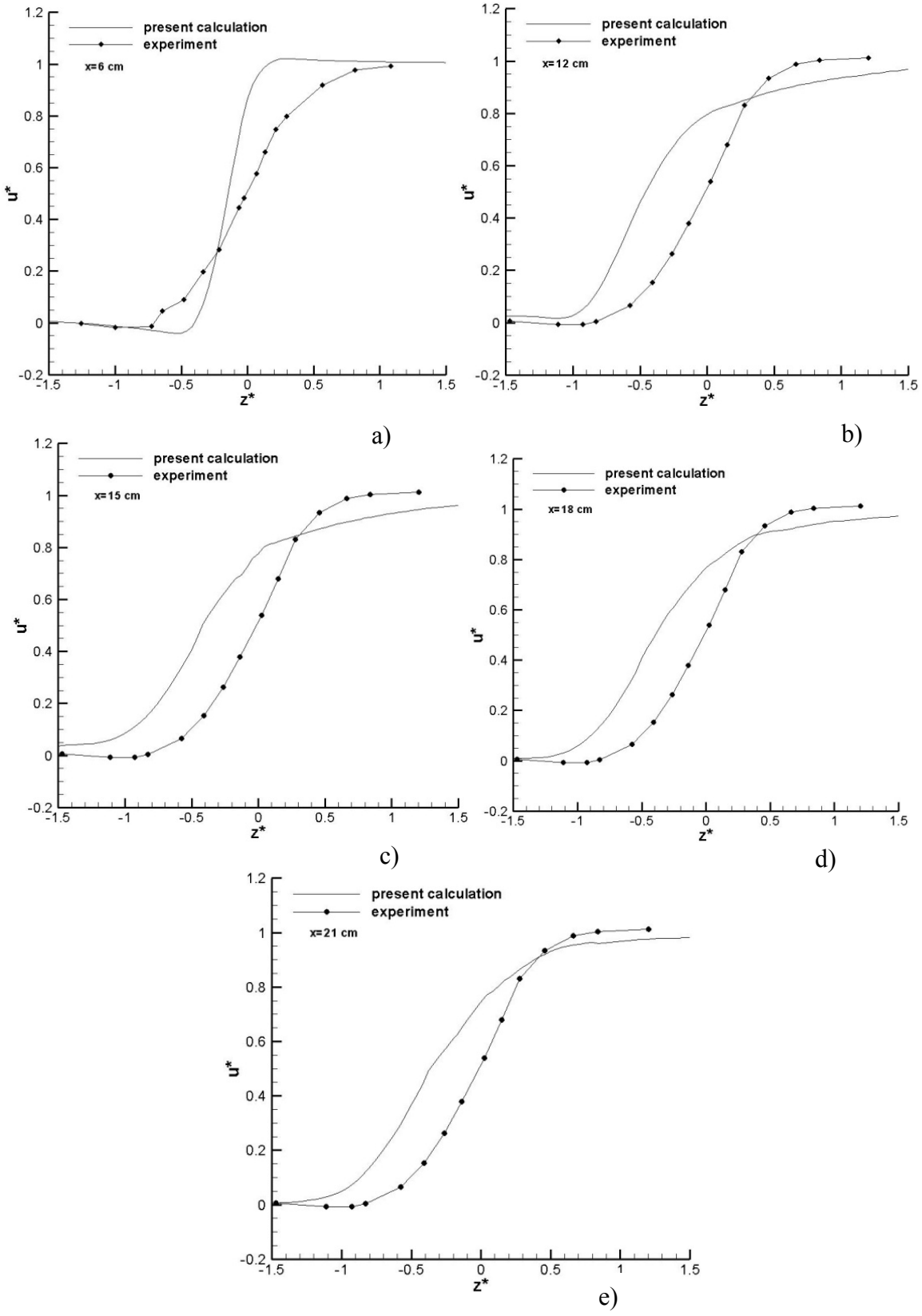

Figure 3 – Comparison of present calculation with experimental data by longitudinal mean velocity profiles at five longitudinal positions in the shear layer
a) x=6, b) x=12, c) x=15, d) x=18, e) x=21 cm.

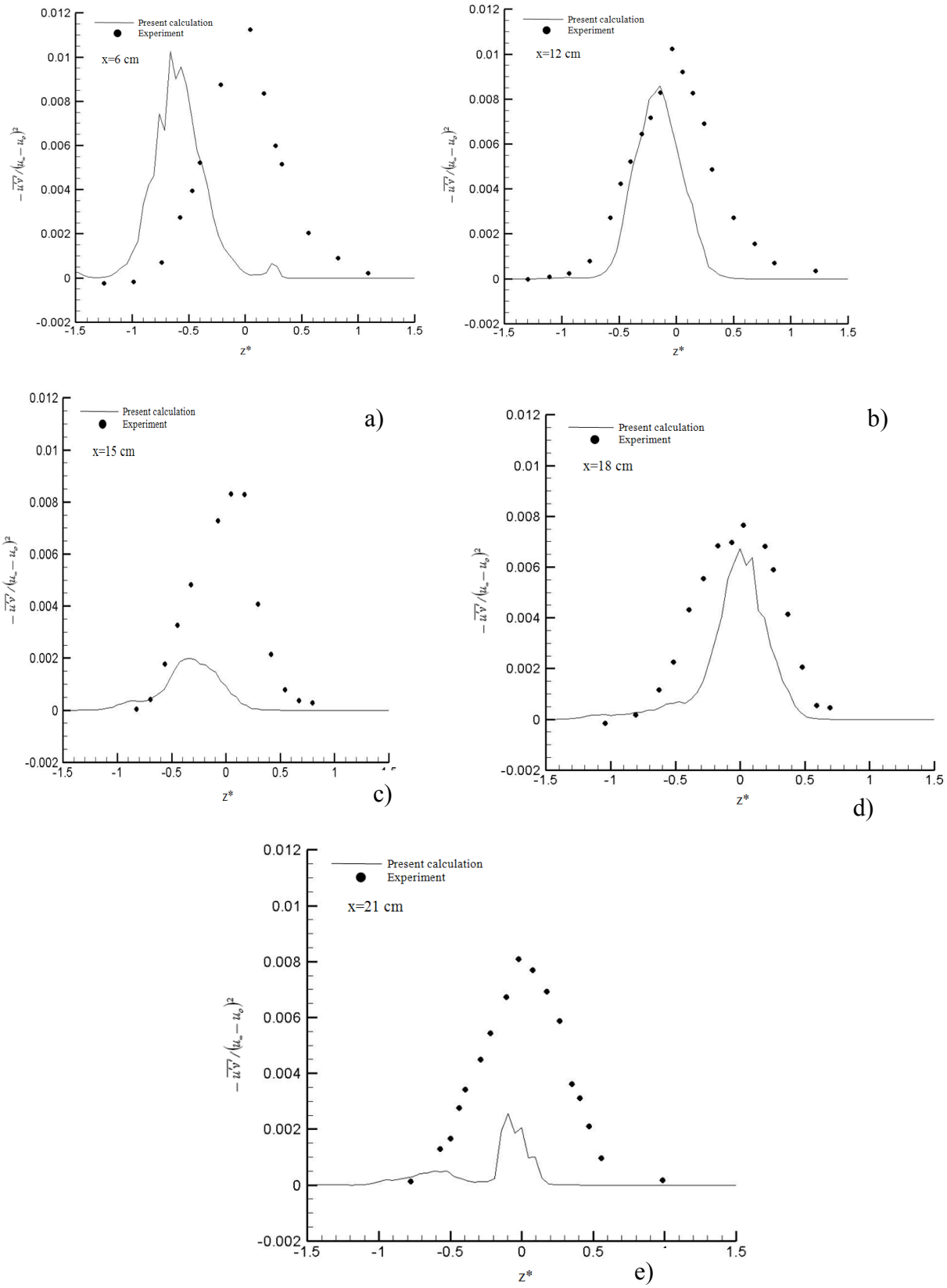

Figure 4 – Comparison of present calculation with experimental data by Reynolds stress at five longitudinal positions in the shear layer a) x=6, b) x=12, c) x=15, d) x=18, e) x=21 cm.

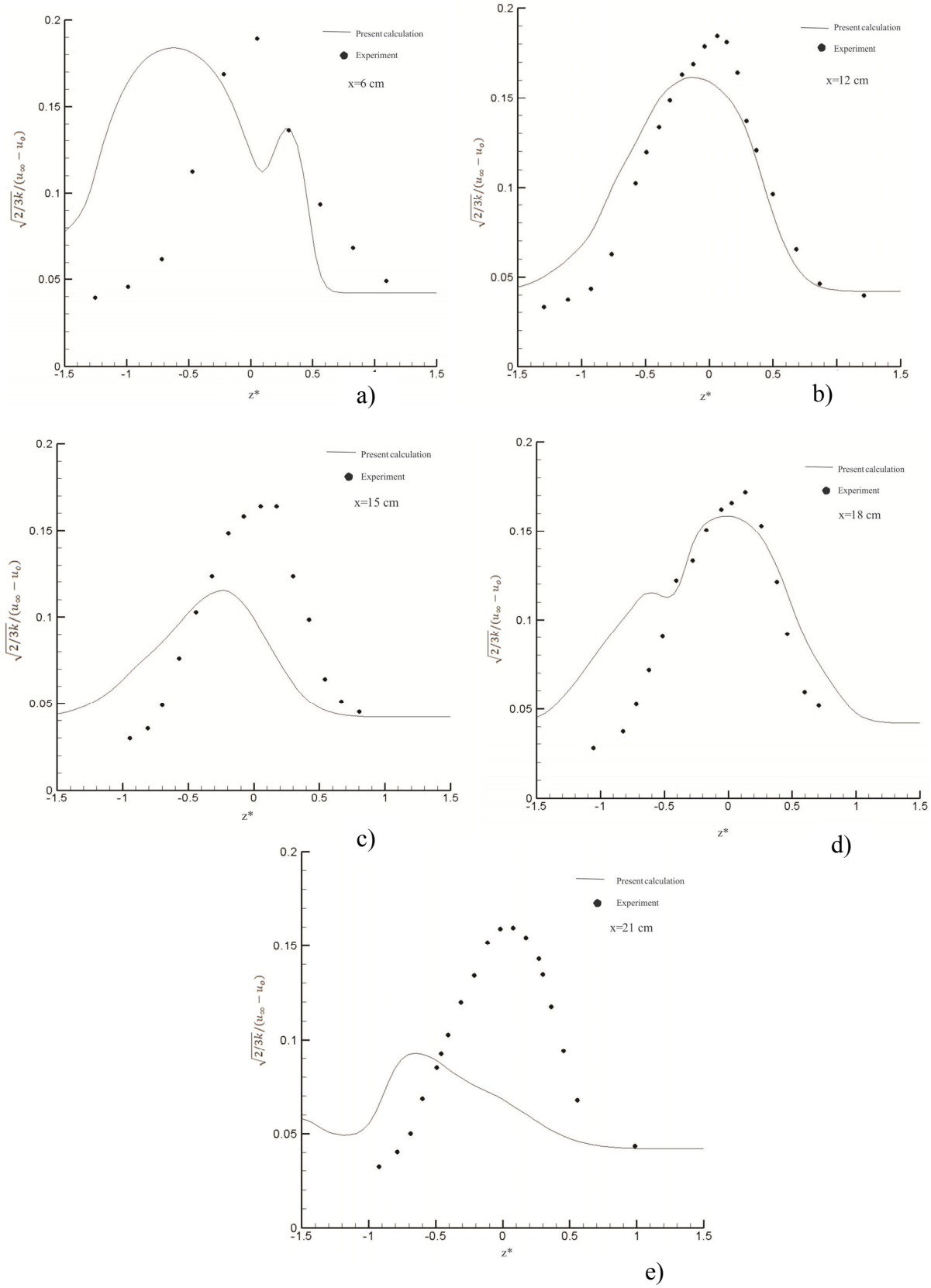

Figure 5 – Comparison of present calculation with experimental data by turbulent intensity at five longitudinal positions in the shear layer a) x=6, b) x=12, c) x=15, d) x=18, e) x=21 cm.

thod with inflow perturbation for prediction of the flowfield structures obtained in experiments. Numerical experiments of influence of unsteady inflow perturbations on the mixing in supersonic free shear layers on the basis of second and fourth order MacCormack scheme have been performed by authors [13-14]. Their studies revealed that normal velocity perturbation is more efficient than streamwise and spanwise. To date rarely performed the numerical investigation of growth of instabilities in shear layer using unsteady disturbances for multispecies gas mixture. In these works have accurately predicted the gas-dynamical structure of shear layers by advanced numerical methods without chemical reactions terms.

In the present study, the third order essentially non-oscillatory (ENO) finite difference scheme is adopted to solve the system of Favre-averaged Navier-Stokes equations to supersonic planar shear layer. The k-ε two-equation turbulence model with compressibility correction is used to predict the turbulence characteristics. To verify the mathematical model and numerical algorithm obtained results compared with experimental study of Samimy and Elliot [8-9] for supersonic-subsonic free shear layer.

The inflow physical parameters profile across the non-premixed hydrogen (fuel) and air stream at the splitter plate leading edge is assumed to vary smoothly according to a hyperbolic-tangent function (Fig. 1).

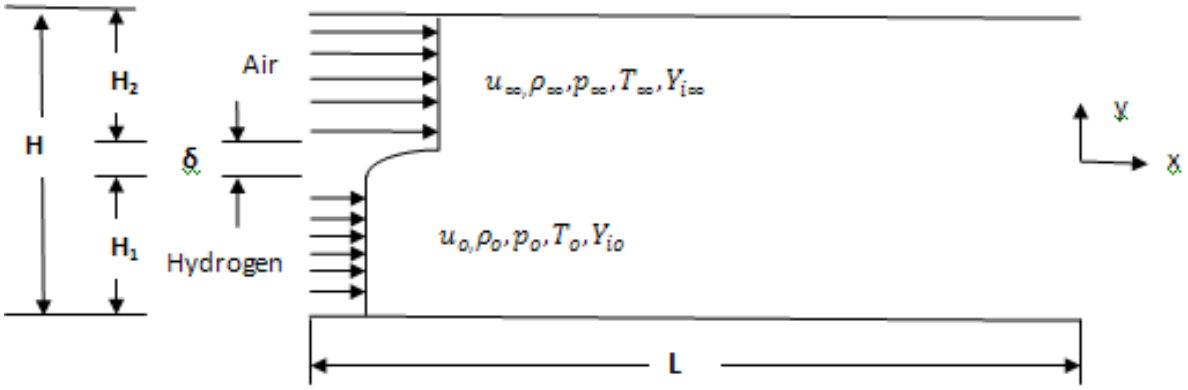

Figure 1 – An illustration of the flow configuration

Mathematical model

The two-dimensional Favre-averaged Navier-Stokes equations for multi-species flow with chemical reactions is:

$$\frac{\partial \vec{U}}{\partial t}+\frac{\partial\left(\vec{E}-\vec{E}_v\right)}{\partial x}+\frac{\partial\left(\vec{F}-\vec{F}_v\right)}{\partial z}=0, \qquad (1)$$

where the vector of the dependent variables and the vector fluxes are given as

$$\vec{U}=\begin{pmatrix}\rho\\ \rho u\\ \rho w\\ E_t\\ \rho Y_k\\ \rho k\\ \rho\varepsilon\end{pmatrix},\quad \vec{E}=\begin{pmatrix}\rho u\\ \rho u^2+p\\ \rho uw\\ (E_t+p)u\\ \rho uY_k\\ \rho uk\\ \rho u\varepsilon\end{pmatrix},\quad \vec{F}=\begin{pmatrix}\rho w\\ \rho uw\\ \rho w^2+p\\ (E_t+p)w\\ \rho wY_k\\ \rho wk\\ \rho w\varepsilon\end{pmatrix},$$

$$\vec{E}_v = \left(0, \tau_{xx}, \tau_{xz}, u\tau_{xx} + w\tau_{xz} - q_x, J_{kx}, \frac{1}{\mathrm{Re}}\left(\mu_l + \frac{\mu_t}{\sigma_k}\right)\frac{\partial k}{\partial x}, \frac{1}{\mathrm{Re}}\left(\mu_l + \frac{\mu_t}{\sigma_\varepsilon}\right)\frac{\partial \varepsilon}{\partial \mathrm{x}}\right)^T,$$

$$\vec{F}_v = \left(0, \tau_{xz}, \tau_{zz}, u\tau_{xz} + w\tau_{zz} - q_z, J_{kz}, \frac{1}{\mathrm{Re}}\left(\mu_l + \frac{\mu_t}{\sigma_k}\right)\frac{\partial k}{\partial z}, \frac{1}{\mathrm{Re}}\left(\mu_l + \frac{\mu_t}{\sigma_\varepsilon}\right)\frac{\partial \varepsilon}{\partial z}\right)^T,$$

$$\vec{W} = \left(0,0,0,0,0, \left[P_k - \rho\varepsilon\left(1 + \alpha M_t^2\right) + D\right], \left[C_{\varepsilon 1} P_k \varepsilon / k - C_{\varepsilon 2} f_{\varepsilon 2} \rho\varepsilon^2 / k\right]\right)^T$$

Here, the viscous stresses, thermal conduction, and diffusion flux of species are:

$$\tau_{xx} = \frac{1}{\mathrm{Re}}\left(\mu_l + \frac{\mu_t}{\sigma_k}\right)\left(2u_x - \frac{2}{3}\left(u_x + w_z\right)\right); \quad \tau_{zz} = \frac{1}{\mathrm{Re}}\left(\mu_l + \frac{\mu_t}{\sigma_k}\right)\left(2w_z - \frac{2}{3}\left(u_x + w_z\right)\right);$$

$$\tau_{xz} = \tau_{zx} = \frac{1}{\mathrm{Re}}\left(\mu_l + \frac{\mu_t}{\sigma_k}\right)\left(u_z + w_x\right);$$

$$q_x = \frac{1}{\mathrm{Pr}\,\mathrm{Re}}\left(\mu_l + \frac{\mu_t}{\sigma_k}\right)\frac{\partial T}{\partial x} + \frac{1}{\gamma_\infty M_\infty^2}\sum_{k=1}^{N} h_k J_{xk}; \quad q_z = \frac{1}{\mathrm{Pr}\,\mathrm{Re}}\left(\mu_l + \frac{\mu_t}{\sigma_k}\right)\frac{\partial T}{\partial z} + \frac{1}{\gamma_\infty M_\infty^2}\sum_{k=1}^{N} h_k J_{zk};$$

$$J_{kx} = -\frac{1}{Sc\,\mathrm{Re}}\left(\mu_l + \frac{\mu_t}{\sigma_k}\right)\frac{\partial Y_k}{\partial x}, \quad J_{kz} = -\frac{1}{Sc\,\mathrm{Re}}\left(\mu_l + \frac{\mu_t}{\sigma_k}\right)\frac{\partial Y_k}{\partial z}.$$

Parameters of the turbulence are:

$$P_k = \tau_{txx}\frac{\partial u}{\partial x} + \tau_{txz}\frac{\partial u}{\partial z} + \tau_{tzx}\frac{\partial w}{\partial x} + \tau_{tzz}\frac{\partial w}{\partial z};$$

$$\tau_{txx} = \frac{\mu_t}{\mathrm{Re}}\left(2\frac{\partial u}{\partial x} - \frac{2}{3}\left(\frac{\partial u}{\partial x} + \frac{\partial w}{\partial z}\right)\right); \quad \tau_{txz} = \frac{\mu_t}{\mathrm{Re}}\left(\frac{\partial u}{\partial z} + \frac{\partial w}{\partial x}\right);$$

$$\tau_{tzz} = \frac{\mu_t}{\mathrm{Re}}\left(2\frac{\partial w}{\partial z} - \frac{2}{3}\left(\frac{\partial u}{\partial x} + \frac{\partial w}{\partial z}\right)\right);$$

$$M_t^2 = 2 \cdot M_\infty^2 \cdot k / T;$$

$$f_{\varepsilon 2} = 1 - 0.3 \cdot \exp\left(-\mathrm{Re}_t^2\right); \quad \mathrm{Re}_t = \mathrm{Re}\left(\frac{\rho k^2}{\mu_l \varepsilon}\right);$$

$$C_{\varepsilon 1} = 1.44; C_{\varepsilon 2} = 1.92; \sigma_k = 1.0; \sigma_\varepsilon = 1.3,$$

where k, ε – turbulent kinetic energy, rate of dissipation of turbulent kinetic energy. P_k – is turbulence production term, M_t – is the turbulence Mach number.

Y_k – is the mass fraction of k^{th} species, $k = 1 \ldots N$, with N -number a components in a gas mixture. The thermal equation for multi-species gas is:

$$p = \frac{\rho T}{\gamma_\infty M_\infty^2 W}, \quad W = \left(\sum_{k=1}^{N} \frac{Y_k}{W_k} \right)^{-1}, \quad \sum_{k=1}^{N} Y_k = 1 \tag{2}$$

where W_k is the molecular weight of the species.

The equation for a total energy is given by

$$E_t = \frac{\rho h}{\gamma_\infty M_\infty^2} - p + \frac{1}{2}\rho\left(u^2 + w^2\right) \tag{3}$$

The enthalpy of the gas mixture is calculated according to $h = \sum_{k=1}^{N} Y_k h_k$, with specific enthalpy of k^{th} species evaluated suing $h_k = h_k^0 + \int_{T_0}^{T} c_{pk} dT$.

The specific heat at constant pressure for each component c_{pk} is:

$$c_{pk} = C_{pk} / W,$$
$$C_{pk} = \sum_{i=1}^{5} \overline{a}_{ki} T^{(i-1)},$$
$$\overline{a}_{jk} = a_{jk} T_\infty^{\,j-1}$$

where the molar specific heat C_{pk} is given in terms of the fourth degree polynomial with respect to temperature, consistent with the JANAF Thermochemical Tables [28].

The system of the equations (1) is written in the conservative, dimensionless form. The air flow parameters are $\rho_\infty, u_\infty, w_\infty, T_\infty, h_\infty, W_\infty, R_\infty$, hydrogen jet parameters are $\rho_0, u_0, w_0, T_0, h_0, W_0, R_0$. The governing parameters are the air flow parameters, the pressure and total energy are normalized by $\rho_\infty u_\infty^2$, the enthalpy by $R_0 T_\infty / W_\infty$, the molar specific heat by R_0 and the spatial distances by the thickness of the splitter plate δ.

The coefficient of viscosity is represented in the form of the sum of μ_l - molecular viscosity and μ_t - turbulent viscosity: $\mu = \mu_l + \mu_t$, where μ_t is defined according to k-ε model with compressibility correction. The mixture averaged molecular viscosity is evaluated using from Wilke's formula.

Initial and boundary conditions

At the entrance:

$$u_1 = M_0 \sqrt{\frac{\gamma_0 R_0 T_0}{W_0}}, \; w_1 = 0, \; p_1 = p_0, \; T_1 = T_0, \; Y_{k1} = Y_{k0}, \; k = k_0, \; \varepsilon = \varepsilon_0 \;\text{ at } x = 0, \quad 0 \le z < \mathrm{H}_1.$$

$$u_2 = M_\infty \sqrt{\frac{\gamma_\infty R_0 T_\infty}{W_\infty}}, \; w_2 = 0, \; p_2 = p_\infty, \; T_2 = T_\infty, \; Y_{k2} = Y_{k\infty}, \; k = k_\infty, \; \varepsilon = \varepsilon_\infty \text{ at } x = 0, \quad \mathrm{H}_1 + \delta \le z \le \mathrm{H}_2.$$

In the region of $\mathrm{H}_1 \le z \le \mathrm{H}_1 + \delta$ all physical variables are varied smoothly from fuel flow to air flow using a hyperbolic-tangent function of any variable φ, so the inflow profiles are defined by

$$\phi(\mathrm{z}) = 0.5\left(\phi_2 + \phi_1\right) + 0.5\left(\phi_2 - \phi_1\right)\tanh\left(0.5 z / \theta\right) \text{ at } x = 0, \quad 0 \le z \le H.$$

where $\phi = (u, v, p, T, Y_k, k, \varepsilon)$, θ - is the momentum thickness. The pressure is assumed to be uniform across the shear layer. On the lower and upper boundary the condition of symmetry are imposed. At the outflow, the non-reflecting boundary condition is used [29].

In order to produce the roll-up and pairing of vortex rings, an unsteady boundary condition is also applied at the inlet plane, i.e.

$$u = u(z) + A\Delta U Gaussian\ (z)\cos(\omega t)$$
$$w = \Delta w_{factor} A\Delta U Gaussian(z)\sin(\omega t)$$
$$Gaussian(z) = \exp(-z^2 / 2\sigma^2),$$

where $u(z)$ - velocity profile at the entrance corresponding to hyperbolic-tangent function. The unsteady part of the condition is about 0.2-0.3 percent of the Favre-averaged velocity. $\Delta U = (u_\infty - u_0)$ - the difference of two stream velocities which measures the strength of shearing. $Gaussian\ (z)$ - is a Gaussian function which has a peak value of unity at z=0 and the $\pm 2\sigma$ width was matched to the vorticity layer thickness at the entrance. Coefficient A is the disturbance amplitude which is defined from the $A \cdot \Delta U$, where this product was specified to be 0.2-0.3 percent of the higher inflow speed. The Δw_{factor} was set at 0.7 (70%) of $A \cdot \Delta U$ based on [16].

The $\omega = 2\pi \left(\frac{\left(\sqrt{\frac{\gamma_0 R_0 T_0}{W_0}} + \sqrt{\frac{\gamma_\infty R_\infty T_\infty}{W_\infty}} \right)/2}{2\delta_w} \right)$ is the frequency of perturbation. $\delta_w = \frac{(u_\infty - u_0)}{(\partial u / \partial z)_{\max}}$ - is the vorticity thickness.

Method of solution

To take into account the flow in the shear (at the entrance) and mixing layer, i.e., in regions of high gradients, more accurately, we refine the grid in the longitudinal and transverse directions by the transformations

$$\frac{\partial \widetilde{U}}{\partial t} + \frac{\partial \widetilde{E}}{\partial \xi} + \frac{\partial \widetilde{F}}{\partial \eta} = \frac{\partial \widetilde{E}_{v2}}{\partial \xi} + \frac{\partial \widetilde{E}_{vm}}{\partial \xi} + \frac{\partial \widetilde{F}_{v2}}{\partial \eta} + \frac{\partial \widetilde{F}_{vm}}{\partial \eta}, \tag{4}$$

where $\widetilde{U} = \vec{U}/J$, $\widetilde{E} = \xi_x \vec{E}/J$, $\widetilde{F} = \eta_z \vec{F}/J$, $\widetilde{E}_{v2} = \xi_x \vec{E}_{v2}/J$, $\widetilde{E}_{vm} = \xi_x \vec{E}_{vm}/J$, $\widetilde{F}_{v2} = \eta_z \vec{F}_{v2}/J$, $\widetilde{F}_{vm} = \eta_z \vec{F}_{vm}/J$, and $J = \partial(\xi, \eta)/\partial(x, z)$ is the Jacobian of mapping.

System (4) linearized with respect to the vector U in form:

$$\widetilde{U}^{n+1} + \Delta t \left(\frac{\partial \widetilde{E}^{n+1}}{\partial \xi} + \frac{\partial \widetilde{F}^{n+1}}{\partial \eta} - \frac{\partial \widetilde{E}_{vm}^{n+1}}{\partial \xi} - \frac{\partial \widetilde{E}_{v2}^{n+1}}{\partial \xi} - \frac{\partial \widetilde{F}_{vm}^{n+1}}{\partial \eta} - \frac{\partial \widetilde{F}_{v2}{}^{n+1}}{\partial \eta} \right) = \widetilde{U}^n + O(\Delta t^2). \tag{5}$$

Here,

$$\widetilde{E}^{n+1} \approx A_\xi^n \widetilde{U}^{n+1},\ \widetilde{F}^{n+1} \approx B_\eta^n \widetilde{U}^{n+1}, \tag{6}$$

$A_\xi = \xi_x A$, $B_\eta = \eta_z B$, $A = \partial \vec{E} / \partial \vec{U}$, $B = \partial \vec{F} / \partial \vec{U}$ - are the Jacobian matrices [32-33].

The terms containing the second derivatives are presented as sums of two vectors:

$$\widetilde{E}_{v2}^{n+1} = \widetilde{E}_{v21}^{n+1} + \widetilde{E}_{v22}^{n}\ , \quad \widetilde{F}_{v2}^{n+1} = \widetilde{F}_{v21}^{n+1} + \widetilde{F}_{v22}^{n}\,, \tag{7}$$

where the vectors $\widetilde{E}_{v21}^{n+1}$, $\widetilde{F}_{v21}^{n+1}$ are written in the following form:

$$\widetilde{E}_{v21}^{n+1} = \frac{\mu_t \xi_x}{\mathrm{Re}\, J}\left[0, \frac{4}{3}\frac{\partial}{\partial\xi}\left(\frac{u\rho}{\rho}\right)^{n+1}, \frac{\partial}{\partial\xi}\left(\frac{w\rho}{\rho}\right)^{n+1}, \frac{\gamma}{\mathrm{Pr}}\frac{\partial}{\partial\xi}\left(\frac{E_t}{\rho}\right)^{n+1}\right]^T,$$

$$\widetilde{F}_{v21}^{n+1} = \frac{\mu_t \eta_z}{\mathrm{Re}\, J}\left[0, \frac{\partial}{\partial\eta}\left(\frac{u\rho}{\rho}\right)^{n+1}, \frac{4}{3}\frac{\partial}{\partial\eta}\left(\frac{w\rho}{\rho}\right)^{n+1}, \frac{\gamma}{\mathrm{Pr}}\frac{\partial}{\partial\eta}\left(\frac{E_t}{\rho}\right)^{n+1}\right]^T,$$

and the vectors $\widetilde{E}_{v12}^{n}$, $\widetilde{F}_{v22}^{n}$ contain the remaining dissipative functions of the form:

$$\widetilde{E}_{v12}^{n} = \frac{\xi_x^2}{\mathrm{Re}\, J}\left[0,0,0, \left[\left(\mu - \frac{\gamma\mu}{\mathrm{Pr}}\right)\left(w\frac{\partial w}{\partial\xi}\right) + \left(\frac{4}{3}\mu - \frac{\gamma\mu}{\mathrm{Pr}}\right)u\frac{\partial u}{\partial\xi}\right]^n\right]^T,$$

$$\widetilde{F}_{v22}^{n} = \frac{\eta_z^2}{\mathrm{Re}\, J}\left[0,0,0, \left[\left(\mu - \frac{\gamma\mu}{\mathrm{Pr}}\right)\left(u\frac{\partial u}{\partial\eta}\right) + \left(\frac{4}{3}\mu - \frac{\gamma\mu}{\mathrm{Pr}}\right)w\frac{\partial w}{\partial\eta}\right]^n\right]^T,$$

$$\widetilde{E}_{vm} = \frac{\xi_x \mu_t}{\mathrm{ReJ}}\left[0, -\frac{2}{3}\left(\eta_z\frac{\partial w}{\partial\eta} + \zeta_y\frac{\partial v}{\partial\zeta}\right), \eta_z\frac{\partial u}{\partial\eta}, -\frac{2}{3}\left(\zeta_y u\frac{\partial v}{\partial\zeta} + \eta_z u\frac{\partial w}{\partial\eta}\right) + \right.$$
$$\left. + \left(\eta_z w\frac{\partial u}{\partial\eta} + \zeta_y v\frac{\partial u}{\partial\zeta}\right)\right],$$
$$\widetilde{F}_{vm} = \frac{\eta_z \mu_t}{\mathrm{ReJ}}\left[0, \eta_z\frac{\partial w}{\partial\eta}, -\frac{2}{3}\left(\xi_x\frac{\partial u}{\partial\xi} + \zeta_y\frac{\partial w}{\partial\zeta}\right), \left(\xi_x u\frac{\partial w}{\partial\xi} + \zeta_y u\frac{\partial w}{\partial\zeta}\right) - \right.$$
$$\left. - \frac{2}{3}\left(\xi_x w\frac{\partial u}{\partial\xi} + \zeta_y w\frac{\partial v}{\partial\zeta}\right)\right].$$

According to a principle of construction ENO scheme [30-31] the system (5) for integration on time is formally represented as:

$$\Delta\widetilde{U}^{n+1} + \Delta t\left[\left(A^+ + A^-\right)\frac{\partial\vec{E}^m}{\partial\xi} + \left(B^+ + B^-\right)\frac{\partial\vec{F}^m}{\partial\eta} - \right.$$
$$\left. \left[\frac{\partial(\widetilde{E}_{v2}{}^{n+1} + \widetilde{E}_{vm}{}^{n})}{\partial\xi} - \frac{\partial(\widetilde{F}_{v2}{}^{n+1} + \widetilde{F}_{vm}{}^{n})}{\partial\eta}\right]\right] = O\left(\tfrac{1}{2}\Delta t^2\right) \tag{8}$$

Here $\vec{E}^m$, $\vec{F}^m$ is called the modified flux vector. It consists from the original flux vector ($\widetilde{E}$, $\widetilde{F}$ and additional terms of third-order accuracy $\vec{E}_\xi, \vec{D}_\xi$, $\vec{E}_\eta, \vec{D}_\eta$) :

$$\vec{E}^m = \widetilde{E}^{n+1} + (\vec{E}_\xi + \vec{D}_\xi)^n\ , \tag{9}$$

modified flux $\vec{F}^m$ is written similarly and $A^+ + A^- = I$, $A^{\pm} = A^{\pm} A^{-1}$, $B^{\pm} = B^{\pm} B^{-1}$, I - unity matrix.

Applying factorization to (8), we obtain two one-dimensional operators, which are resolved by matrix sweep:

Step 1:

$$\left[I + \Delta t \left\{ (A^+_{i-1/2} \Delta_- A^n_\xi + A^-_{i+1/2} \Delta_+ A^n_\xi) + \Delta \frac{\mu_t \xi_x^2}{\mathrm{Re}\, J} \Delta \frac{1}{U_1^n} \right\} \right] \mathrm{U}^* = RHS^n_\xi + RHS^n_\eta$$

Step 2:

$$\left[I + \Delta t \left\{ (B^+_{j-1/2} \Delta_- B^n_\eta + B^-_{j+1/2} \Delta_+ B^n_\eta) + \Delta \frac{\mu_t \eta_z^2}{\mathrm{Re}\, J} \Delta \frac{1}{U_1^n} \right\} \right] \tilde{\mathrm{U}}^{n+1} = \mathrm{U}^*, \tag{10}$$

$$RHS^n_\xi = A^-_{i+1/2j} \left[\left(\vec{E}_\xi + \vec{D}_\xi \right)_{i+1j} - \left(\vec{E}_\xi + \vec{D}_\xi \right)_{ij} \right]^n + A^+_{i-1/2j} \left[\left(\vec{E}_\xi + \vec{D}_\xi \right)_{ij} - \left(\vec{E}_\xi + \vec{D}_\xi \right)_{i-1j} \right]^n,$$

$$A^-_{i+1/2j} \left[\left(\vec{E}_\zeta + \vec{D}_\zeta \right)_{ij} \right]^n = \left(\boldsymbol{minmod} \left(\overline{E}_{\xi i+1/2j}\ \overline{E}_{\xi i-1/2j} \right) + \right.$$
$$\left. + \begin{cases} \dot{\boldsymbol{m}} \left(\Delta_- D_{\xi i+1/2j},\ \Delta_+ D_{\xi i+1/2j} \right) & \text{if} \quad \left| \Delta_- \tilde{U}_{ij} \right| > \left| \Delta_+ \tilde{U}_{ij} \right| \\ \dot{\boldsymbol{m}} \left(\Delta_- \overline{D}_{\xi i-1/2j},\ \Delta_+ \overline{D}_{\xi i-1/2j} \right) & \text{if} \quad \left| \Delta_- \tilde{U}_{ij} \right| \le \left| \Delta_+ \tilde{U}_{ij} \right| \end{cases} \right],$$

$$A^+_{i-1/2j} \left[\left(\vec{E}_\xi + \vec{D}_\xi \right)_{ij} \right]^n = R \Lambda^+ R^{-1}_{i-1/2j} \left[\left(\boldsymbol{minmod} \left(\overline{E}_{\xi i+1/2j}\ \overline{E}_{\xi i-1/2j} \right) - \right. \right.$$
$$\left. \left. - \begin{cases} \dot{\boldsymbol{m}} \left(\Delta_- D_{\xi i-1/2j},\ \Delta_+ D_{\xi i-1/2j} \right) & \text{if} \quad \left| \Delta_- \tilde{U}_{ij} \right| \le \left| \Delta_+ \tilde{U}_{ij} \right| \\ \dot{\boldsymbol{m}} \left(\Delta_- \overline{D}_{\xi i-1/2j},\ \Delta_+ \overline{D}_{\xi i-1/2j} \right) & \text{if} \quad \left| \Delta_- \tilde{U}_{ij} \right| \le \left| \Delta_+ \tilde{U}_{ij} \right| \end{cases} \right],$$

$$\overline{E}_{\xi i\pm1/2j} = \left(R\, sign\,(\Lambda) R^{-1} \right)_{i\pm1/2j} \frac{1}{2} \left[I - \frac{\Delta t}{\Delta \xi} \left(R\, |\Lambda|\, R^{-1} \right)_{i\pm1/2} \right] \Delta_\pm \tilde{E}_{ij},$$

$$\overline{D}_{\xi i\pm1/2j} = \left(R\, sign\,(\Lambda) R^{-1} \right)_{i\pm1/2j} \frac{1}{6} \left[\frac{\Delta t^2}{\Delta \xi^2} \left(R\, |\Lambda|\, R^{-1} \right)^2_{\pm} - I \right] \Delta_\pm \tilde{E}_{ij},$$

$$D_{\xi i\pm1/2j} = \overline{E}_{\xi i\pm1/2j} + \overline{D}_{\xi i\pm1/2j},$$

where $\boldsymbol{minmod}(a,b) = \begin{cases} s \cdot min(|a|,|b|) & \text{if} \quad sign(a) = sign(b) = s \\ 0 & \text{other} \end{cases}$,

$$\dot{\boldsymbol{m}}(a,b) = \begin{cases} a & \text{if} \quad |a| \le |b| \\ b & \text{if} \quad |a| > |b| \end{cases}.$$

The second term $RHS^n{}_\eta$ is written similarly.

In approximation of derivatives in convective and diffusion terms, we use second-order central-difference operators.

The numerical solution of the system (5) is calculated in two steps. The first determines the dynamic parameters and second determines the mass species.

Then it is necessary to define Jacobian matrix which in a case of the thermally perfect gas represents difficult task. This problem is connected with the explicit representation of pressure through the unknown parameters. Here pressure is determined by introducing an effective adiabatic parameter of the gas mixture [34].

$$\bar{\gamma} = \frac{h_{sm}}{e_{sm}} \ , \qquad (11)$$

where $h_{sm} = \sum_{i=1}^{N} Y_i \int_{T_0}^{T} c_{p_i} dT$, $e_{sm} = \sum_{i=1}^{N} Y_i \int_{T_0}^{T} c_{v_i} dT$ – is the enthalpy and internal energy of the mixture minus the heat and energy of formation; $T_0 = 293\ K$ - is the standard temperature of formation, which allows to write an expression for the pressure

$$p = (\bar{\gamma} - 1)\left[E_t - \frac{1}{2}\rho\left(u^2 + w^2\right) - \rho \frac{h_0}{\gamma_\infty M_\infty^2} \right] + \frac{\rho T_0}{M_\infty^2 W} \cdot$$

The temperature is found from the Newton-Raphson iteration [32-33, 35].

The equations for species are solved by the scalar sweep, where in the first-step convection and diffusion terms are included and calculated using ENO scheme [30-31]. In the second-step, the matrix equation with terms ($\dot{w}_k = W_k \dot{\omega}_k$) is solved implicitly. These source terms $\dot{W}_k$ are linearized by expansion in a Taylor series,

$$\dot{W}_k^{n+1} = \dot{W}_k^{n} + \gamma\left(\frac{\partial \dot{W}_k}{\partial Y_m} \Delta Y_m + \frac{\partial \dot{W}_k}{\partial T} \Delta T + \frac{\partial \dot{W}_k}{\partial \rho} \Delta \rho \right)$$

Results and discussion

The parameters of coordinate transformation have the form:

$$\xi(x) = H \left[(\beta+1) - (\beta-1)\left(\frac{\beta+1}{\beta-1} \right)^{1 - \frac{x}{L}} \right] \Bigg/ \left[\left(\frac{\beta+1}{\beta-1} \right)^{1-\frac{x}{L}} + 1 \right],$$

$$\eta(z) = K + \frac{1}{\tau} arsh\left[\left(\frac{z}{z_c} - 1 \right) sh(\tau K) \right],$$

$$K = \frac{1}{2\tau} \ln\left[\left(1 + (e^{\tau} - 1)\frac{z_c}{H} \right) \Bigg/ \left(1 - (e^{\tau} - 1)\frac{z_c}{H} \right) \right],$$

β, τ are refinement factors (β>1 and τ >1), L - is the length of the computational domain in the generalized coordinates, and z_c - is the point with respect to which grid refinement is performed.

Previously the shear layer problem for monatomic (air) gas has been tested by the following parameters:

$M_0 = 0.51,\ T_0 = 285.07\ K,\ P_0 = 56088.91\ Pa,$

$M_\infty = 1.8,\ T_\infty = 176.58\ K,\ P_\infty = 54648.65\ Pa.$

The computational grid is 526x201. The channel height and length were 8 cm and 50 cm, respectively. The splitter plate thickness is 0.3175 cm, and at the trailing edge is 0.05 cm. The initial momentum thickness $\theta = \int_{-\infty}^{+\infty} \left(\frac{\rho}{\rho_\infty} u^* \left(1 - u^*\right) dz \right)$ is 0.05 cm. The geometrical parameters above are taken from experimental work of Samimy and Elliot [8-9]. Experiment was conducted in tunnel, present calculation performed for planar channel to estimate the behavior of turbulence quantities. Figures 2-4 shows ($M_c = 0.51$) the comparison of the calculated distributions of longitudinal (axial) mean velocity, variation of the momentum (θ) and vorticity (δ_w) thicknesses, and turbulence quantities with the experimental data [8-9]. The non-

dimensional variables $u^* = \frac{(u-u_0)}{(u_\infty - u_0)}$, $z^* = \frac{(z-z_c)}{\delta_w}$, $\theta = \int_{-\infty}^{+\infty}\left(\frac{\rho}{\rho_\infty}u^*(1-u^*)dz\right)$, $\delta_w = \frac{(u_\infty - u_0)}{(\partial u/\partial z)_{\max}}$ are defined as in the experiments [8-9]. Figure 2 indicates that the shear layer growth in terms of momentum and vorticity thickness is predicted reasonably accurate by the present algorithm, as compared to experimental data.

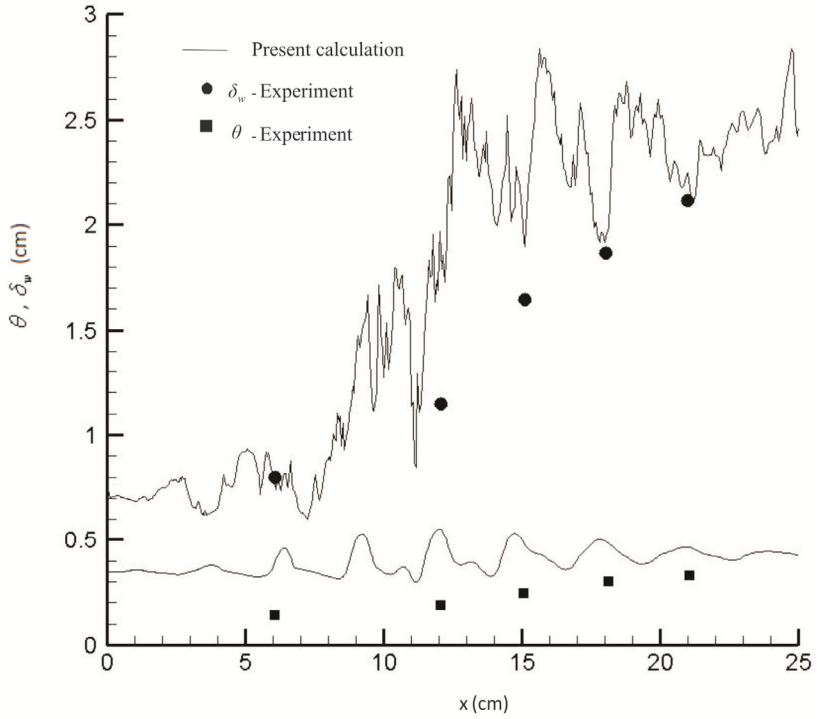

Figure 2 – Comparison of present calculation with experimental data by the growth of momentum and vorticity thickness.

The comparison of calculated transverse distribution of the normalized streamwise mean velocity at five longitudinal positions with experimental measurements as shown in Figure 3 suggest that in the fully developed region for x≥12 cm the mean flow is self-similar.

Further comparison of the calculated results with experimental data are shown for the development of the Reynolds stress $-\overline{u'v'}/(u_\infty - u_o)^2$ in Figures 4 and streamwise turbulence intensity $\sqrt{2/3k}/(u_\infty - u_o)$ in Figure 5. The contribution of transverse velocity fluctuating component to turbulent kinetic energy was neglected. It is visible from figures that the calculated turbulence quantities are distorted at x≥15 cm, which shows that the turbulence similarity is achieved further downstream than the mean flow similarity. The preliminary test shown that the mean and turbulence quantities are in a good agreement with experimental data.

Conclusion

The flowfield structures of supersonic turbulent planar shear layer computed by calculation of the system of two-dimensional planar Favre-averaged Navier-Stokes equations. The k-ε two-equation turbulence model with compressibility correction is used to determine the eddy viscosity coefficient. The numerical method is based on the third order ENO finite-difference scheme. The comparison of present results obtained by using ENO scheme and k-ε turbulence model with experimental data demonstrates a satisfactory prediction of mean and turbulence properties of the flow.

Thus the constructed algorithm based on the high order scheme and computer code for turbulent supersonic flow allows to study influence parameters that control mixing, which is important in the design of supersonic combustion ramjet (scramjet) engines and easily expanded into 3D case.

References

1. Winant, C.D., Browand, F.K., 1974. Vortex pairing: the mechanism of turbulent mixing-layer growth at moderate Reynolds number. J. Fluid Mech. 63, P.237-255.

2. Brown, G.L., Roshko, A., 1974. On the density effects and large structures in turbulent mixing layers. J. Fluid Mech. 64, P.775-816.

3. Bogdanoff, D.W., 1983. Compressibility effects in turbulent shear layers. AIAA J.21, P.926-927.

4. Papamoschou, D., Roshko, A., 1988. The compressible turbulent shear layer: an experimental study. J. Fluid Mech. 197, P. 453-477.

5. Chinzei, N., Masuya, G., Komuro, T., Murakami A., Kudou, K., 1986. Spreading of two-stream supersonic turbulent mixing layers. Phys. Fluids 29, P. 1345-1347.

6. Goebel, S. G., Dutton, J.C., 1991. Experimental study of compressible turbulent mixing layers. AIAA Journal 29, 4, P. 538-546.

7. Oster, D., Wygnanski, I., 1982. The forced mixing layer between parallel streams. J. Fluid Mech. 123, P. 91-130.

8. Samimy, M., Elliot, G.S., 1990. Effects of compressibility on the characteristics of free shear layers. AIAA J. 28, P.439-445.

9. Elliot, G.S., Samimy, M., 1990. Compressibility effects in free shear layers. Phys. Fluids A 2, P.1231-1240.

10. Ju, Y., Niioka, T., 1993. Ignition Analysis of Unpremixed Reactants with Chain Mechanism in a Supersonic Mixing Layer. AIAA Journal, Vol. 31, No. 5, P. 863-868.

11. Im, H. G., Chao, B. H., Bechtold, J. K., Law, C. K., 1994. Analysis of Thermal Ignition in the Supersonic Mixing Layer. AIAA Journal, Vol. 32, No. 2, P.341-349.

12. Cheng, T.S., Lee, K.S., 2005. Numerical simulations of underexpanded supersonic jet and free shear layer using WENO schemes. International Journal of Heat and Fluid Flow 26, P.755-770.

13. Tang, W., Komerath, N.M., Sankar, L.N., 1990. Numerical simulation of the Growth of instabilities in Supersonic Free Shear Layers. J. Propulsion vol. 6, no. 4, P. 455-460.

14. Tang, W., Sankar, L.N., Komerath, N., 1989. Mixing enhancement in supersonic free shear layers. AIAA 2nd Shear Flow Conference, AIAA 89-0981.

15. Reichert, R.S., Biringen, S., 2007. Numerical simulation of compressible plane jets. Mechanics Research Communications 34, P.249-259.

16. Dale A. Hudson, 1996. Numerical simulation of a confined supersonic shear layer. PhD dissertation, P.1-181.

17. Xiao-Tian Shi, Jun Chen, Wei-Tao Bi, Chi-Wang Shu, Zhen-Su She, 2011. Numerical simulations of compressible mixing layers with a discontinuous Galerkin method. Acta Mech. Sin. 27 (3), P.318-329.

18. Zambon, A.C., Sriram, A.T., Chelliah, H.K., 2007. Development and Implementation of Explicit Reduced Reaction Models in Supersonic Reacting Shear Flow Simulations. 45th AIAA Aerospace Sciences Meeting and Exhibit, Reno, Nevada, AIAA-2007-772.

19. Sriram, A.T., Zambon, A.C., Chelliah, H.K., 2008. Validation of Ethylene-Air Reduced Reaction Models in Supersonic Shear Flows. 46th AIAA Aerospace Sciences Meeting and Exhibit, Reno, Nevada, AIAA-2008-993.

20. Da Silva, L. F. F., Deshaies, B., Champion, M., 1993. Some Specific Aspects of Combustion in Supersonic H2-Air Laminar Mixing Layers. Combustion Science and Technology, Vol. 89, P.317-333.

21. Nishioka, M., Law, C.K., 1997. A Numerical Study of Ignition in the Supersonic Hydrogen/Air Laminar Mixing Layer. Combustion and Flame, Vol. 108, P.199-219.

22. Fang, X., Liu, F., Sirignano, W. A., 2001. Ignition and Flame Studies for an Accelerating Transonic Mixing Layer. Journal of Propulsion and Power. Vol. 17, No. 5, P.1058-1066.

23. Ju, Y., Niioka, T., 1994. Reduced Kinetic Mechanism of Ignition for Nonpremixed Hydrogen/Air in a Supersonic Mixing Layer. Combustion and Flame, Vol. 99, P.240-246.

24. Ju, Y., Niioka, T., 1995. Ignition Simulation of Methane/Hydrogen Mixtures in a Supersonic Mixing Layers. Combustion and Flame, Vol. 102, P.462-470.

25. Tahsini, A.M., 2011. Ignition Analysis in Supersonic Turbulent Mixing Layer. World Academy of Science, Engineering and Technology 57, P. 353-357.

26. Tahsini, A.M., 2012. Ignition Time Delay in Swirling Supersonic Flow Combustion. World Academy of Science, Engineering and Technology 70, P. 623-627.

27. Chakraboty, D., Paul, P. J., Mukunda, H. S., 2000. Evaluation of Combustion Models for High Speed H2/Air Confined Mixing Layer Using DNS Data. Combustion and Flame, Vol. 121, P.195-209.

28. Kee, R. J., Rupley, F. M., Miller, J. A., 1989. CHEMKIN-II: a Fortran chemical kinetic package for the analysis of gas-phase chemical kinetics. SANDIA Report SAND89-8009.

29. Poinsot, T.J., Lele, S.K., 1992. Boundary conditions for direct simulation of compressible viscous flows. Journal of Computational Physics, No. 101, P.104-129.

30. Harten, A., Osher, S., Engquist, B., Chakravarthy, S.R., 1986. Some Results on Uniformly High-Order Accurate Essentially Non-oscillatory Schemes. Applied Num. Math., Vol.2., P.347-377.

31. Yang, J. Y., 1991. Third order nonoscillatory schemes for the Euler equations. AIAA J., Vol. 29, No. 10, P.1611-1618.

32. Bruel, P., Naimanova, A. Zh., 2010. Computation of the normal injection of a hydrogen jet into a supersonic air flow. Thermophysics and Aeromechanics, Vol. 17, No. 4, P.531-542.

33. Belyayev, Ye., Naimanova, A. Zh., 2012. Two-Dimensional Supersonic Flow with Perpendicular Injection of the Gas. Chapter 2 InTech open access book “Advanced Methods for Practical Applications in Fluid Mechanics”, P.23-44.

34. Shuen, J. Sh., Yoon, S., 1989. Numerical study of chemical reacting flows using a lower-upper symmetric successive overrelaxation scheme. AIAA J., Vol. 27, No. 12, P.1752-1760.

35. Belyayev Ye., Kaltayev A., Naimanova A. Zh., 2010. Supersonic Flow with Perpendicular Injection of a Hydrogen. Proceedings of 2010 2nd International Conference on Computer Engineering and Technology, Vol. 5, Mechanical and Aerospace Engineering, V5-531-534.